Gold nanoparticles as drug carriers: a contribution to the quest for basic principles for monolayer design†

Mariangela Boccalon,[a] Silvia Bidoggia,[a] Francesco Romano,[b] Lorenzo Gualandi,[b] Paola Franchi,[b] Marco Lucarini,*[b] Paolo Pengo*[a] and Lucia Pasquato*[a]

Two structurally different water-soluble homoligand gold nanoparticle systems, one featuring a rigid fluorous monolayer in the proximity of the gold core and the other featuring a flexible fluorinated region in a distal position, were studied as putative hosting systems by determining their binding constants for a series of fluorinated and non-fluorinated radical probes by means of ESR spectroscopy. Comparison of the binding constants obtained with hydrogenated homoligand nanoparticles of similar structure used as the reference evidenced that the binding of both hydrogenated and fluorinated guests is favoured in the presence of fluorinated nanoparticles. In addition, a flexible fluorinated monolayer acts as a better hosting system than the more rigid counterpart. In the latter case decreasing the size of the nanoparticles causes a small decrease of the binding affinities for both hydrogenated and fluorinated guests. The same nanoparticle systems were analysed for their ability to retard the phase transfer of a fluorescent dye from an aqueous solution to a toluene layer. All of the nanoparticles studied produced a significant decrease of the phase transfer rate of the dye because of the efficient interaction with the monolayer. These data support the introduction of fluorinated moieties in the monolayer of gold nanoparticles as a novel design tool for the development of drug delivery systems.

Accepted 2nd November 2014

Introduction

The use of nanoparticles as delivery systems for therapeutics has manifold benefits: it allows us to overcome the poor solubility of small molecule drugs in aqueous solutions and by taking advantage of the Enhanced Permeation and Retention (EPR) of neoplastic tissues it provides a mechanism for fast accumulation of the drugs at the target site. In addition, NPs may be coupled with targeting ligands for molecular recognition and their surface tailored to avoid the immunogenic and non-specific interactions that efficiently clear foreign materials from the body. Nanoparticles may also be engineered to allow tracking of the drugs and easily implemented into theranostic platforms.[1–5] With focus on monolayer protected gold nanoparticles, the loading of small molecule drugs may be achieved by covalent and non-covalent binding.[6] In the first case the nanoparticles are used as scaffolds; in the second, the particles, more precisely their monolayers, act as hosting systems. Here a series of weak interactions are expected to trigger the complexation and kinetic trapping of the drug molecules. In the covalent approach the preparation of tethered pro-drugs[7–10] is a prerequisite but in some cases the functionalization of the small molecule drugs may not be trivial. Instead, exploiting non-covalent interactions largely reduces the synthetic efforts on the drug side, with the penalty of requiring a judicious design of the hosting monolayer. Notwithstanding the examples of efficient drug loading and release obtained by this method,[11,12] our present understanding of the principles on the basis of monolayer design for drug transport and delivery by non-covalent interactions remains largely incomplete.[13,14] Indeed, the effect of the monolayer structure on dictating the affinity towards putative drugs is only little analysed. For example, the question whether or not the complexation of drugs triggers structural modifications of the monolayer as the result of the necessary guest desolvation accompanying the recognition event. As a consequence, the number of available strategies allowing the achievement of strong binding and kinetic trapping of the guests suffers from severe limitations. Aiming at specifically analysing how the monolayer structure affects the thermodynamics of the monolayer's host–guest chemistry, we endeavoured to systematically evaluate, by means of ESR spectroscopy, the complexation properties of fluorinated and hydrogenated radical probes with gold nanoparticles displaying fluorous monolayers. The evaluation of the interaction between

[a]Department of Chemical and Pharmaceutical Sciences, University of Trieste, I-34127, Trieste, Italy. E-mail: ppengo@units.it; lpasquato@units.it

[b]Department of Chemistry "G. Ciamician", University of Bologna, I-40126 Bologna, Italy. E-mail: marco.lucarini@unibo.it

† Electronic supplementary information (ESI) available: Synthetic procedures for thiol **8**, characterization of nanoparticles **NP1**, **NP2**, **NP3a** and **NP3b**, and kinetic profiles for the release of **7** by **NP1** and **NP2**. See DOI: 10.1039/c4tb01536c

nanoparticles and fluorinated guests is of relevance in the context of drug delivery because of the large number of antineoplastic drugs featuring one or more fluorine atoms currently approved by the FDA.[15] These drugs display a rich structural diversity: a single fluorine atom is found as a substituent on heterocyclic rings such as in 5-fluorouracile or Fludarabine, or as substituents on aromatic rings (Gefitinib, Lapatinib). Trifluoromethyl groups are found as substituents of aromatic rings in the molecule of Flutamide, Sorafenib, or Nilutamide. Some of these structural features are modelled by the probes selected for this study.

Results and discussion

The set of nanoparticles selected for the study was devised to analyze two aspects of the monolayer design in terms of their impact on the monolayer host–guest chemistry: (1) the effects of a fluorocarbon (perfluoroalkyl chains) shell close to the gold core in comparison with a hydrogenated shell and (2) the effect of introducing a flexible fluorinated region (short perfluoropolyoxoethylene chains) distal to the gold core. In this case we also analysed the effect of the nanoparticle size on the affinity for small organic molecules. In all of the cases, the nanoparticles' monolayer was designed to present on its outer surface a pegylated region to impart solubility in water and to shield the recognition elements from the solvent bulk. The structures of the nanoparticle systems analysed are reported in Scheme 1.

Synthesis and characterization of gold NPs

Gold nanoparticles **NP1** and **NP3a** were prepared following the homogeneous phase synthesis reported by our group.[16] To obtain nanoparticles with an average diameter between 3 and 3.4 nm we employed a 3/2 Au/thiol molar ratio and a slow addition of the reducing agent at 0 °C. To prepare nanoparticles **NP3b**, with a gold core size of 1.4 nm, the homogeneous phase synthesis was carried out with a Au/thiol molar ratio of 1/2 and fast addition of the reducing agent at 0 °C.[17]

Gold nanoparticles **NP2** were synthesized following a homogeneous phase synthesis similar to that used for **NP1**, **NP3a** and **NP3b**. However, in the case of nanoparticles **NP2** the low nucleophilicity of the sulfur atom due to the electron withdrawing effect of the fluorinated chain in the α-position forced us to use the thiolate instead of the thiol.[18] To obtain nanoparticles with a gold core of 3–3.2 nm without the formation of aggregates we used a Au/thiol molar ratio of 2/1 and added the reducing agent slowly at room temperature. In all of the cases increasing the Au/thiol ratio resulted in larger nanoparticles in keeping with previous results.[16,18] The nanoparticles were fully characterized by NMR, UV-Vis spectroscopies, TEM and TGA. The diameters, the organic content and the composition of the nanoparticles **NP1**, **NP2**, **NP3a** and **NP3b** are reported in Table 1.

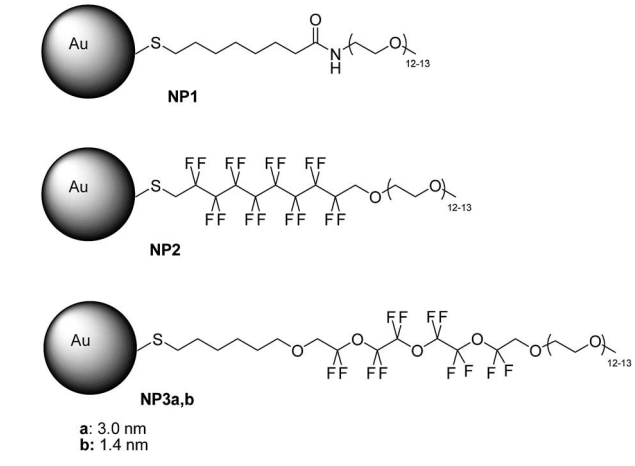

Scheme 1 Structures of the nanoparticles used in this study, the diameter of the gold core of NP3a is 3.0 nm, and the diameter of the gold core of NP3b is 1.4 nm.

Complexation studies by ESR

Complexation studies of hydrogenated and fluorinated radical probes **1–6**, Scheme 2, with fluorinated and hydrogenated homoligand nanoparticles **NP1**, **NP2**, **NP3a** and **NP3b** were carried out in order to assess the relevance of fluorophilic interactions in the molecular recognition events. The radical probes we have used in this study belong to a family of *para*-substituted benzyl hydroxyalkyl nitroxides.

They were generated directly inside an ESR tube by oxidizing the parent secondary amines (**1H–6H**, 0.5 mM) with Oxone (0.5 mM) both in the absence and in the presence of different amounts of nanoparticles. Amines **1H** and **3H** were prepared as already reported,[13,14] while amine precursors **4H–6H** were prepared by reacting 2-amino-2-methyl-1-propanol with the appropriately substituted benzaldehyde followed by reduction with 2 equivalents of $NaBH_4$ (see the Experimental section).

Good ESR spectra of nitroxides **1–6** in water were obtained in all cases by oxidation of the corresponding amines. As an example, Fig. 1a reports the spectrum obtained by oxidizing amine **5H** in water at 298 K. All spectra were easily interpreted on the basis of the coupling of the unpaired electron with nitrogen $a(N)$, and with the two benzylic protons $a(H_\beta)$ (see Table 2).‡ With nitroxide **6**, unresolved coupling with fluorine atoms gives rise to a significant broadening of the ESR lines compared to the other nitroxides.

When the ESR spectra of radicals **1–6** were recorded in the presence of nanoparticles, additional signals were observed, assigned to the radical partitioned in the organic monolayer of the nanoparticle, in equilibrium with the free nitroxide. As an example, Fig. 1b reports the spectrum of **5** recorded in the presence of 1.3 mM **NP3b**. By increasing the absolute concentration of nanoparticles, it was possible to increase the amount of the included radical which in most cases became the

‡ Nitroxide **5** shows significantly larger $a(H_\beta)$ coupling compared to the other nitroxides. This should be attributed to the presence of bulkier fluorine atoms at the *ortho* position which are expected to increase the weight of conformations where the dihedral angle between the benzylic hydrogen and the symmetry axis of the $2p^{\pi}$-orbital containing the unpaired electron is close to 30°.

Table 1 Diameters determined by TEM and TGA analyses, and average composition of the nanoparticles **NP1**, **NP2**, **NP3a** and **NP3b**

Nanoparticles	Diameter (nm)	Organic content (%)	Average composition[a]
NP1	3.4 ± 0.6	40	$Au_{1414}(SR)_{270}$
NP2	3.0 ± 0.6	39	$Au_{976}(SR)_{120}$
NP3a	3.0 ± 0.7	62	$Au_{976}(SR)_{187}$
NP3b	1.4 ± 0.3	84	$Au_{100}(SR)_{60}$

[a] Determined by the combination of the TEM and TGA analyses.

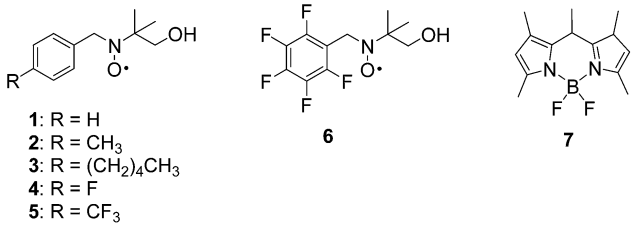

1: R = H
2: R = CH_3
3: R = $(CH_2)_4CH_3$
4: R = F
5: R = CF_3

6 **7**

Scheme 2 Structures of the radical and fluorescent probes used in this study.

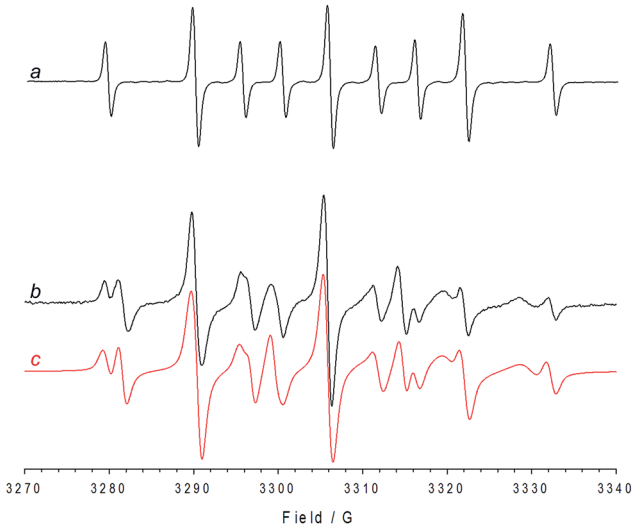

Fig. 1 ESR spectra of **5** recorded at 298 K in water (a) and in the presence of **NP3b** 1.3 mM (b). In red is reported the corresponding computer simulation (c).

Table 2 ESR parameters of nitroxides **1–6** (1 G = 0.1 mT) and equilibrium constants for their partition in nanoparticle monolayers and SDS micelles in water at 298 K

Nitroxide	Phase	a(N)/G	$a(2H_\beta)$/G	K_{eq}[a]/M^{-1}
1	H_2O	16.17	10.43	—
	NP3a	15.31	8.69	6.2
	NP3b	15.37	8.65	4.0
	SDS	15.73	9.06	20
2	H_2O	16.21	10.48	—
	NP3a	15.54	8.89	16
	NP3b	15.52	8.93	11
	NP2	15.60	9.30	5.7
	NP1	15.20	8.50	2.2
	SDS	15.73	8.84	44
3	H_2O	16.25	10.14	—
	NP3b	15.45	8.65	593[b]
	NP2	15.46	8.68	176[c]
	NP1*	15.67	8.97	104[d]
	NP1**	15.70	9.00	77.6[d]
4	H_2O	16.20	10.68	—
	NP3a	15.34	8.77	11
	NP3b	15.38	8.76	8.3
5	H_2O	16.02	10.42	—
	NP3a	15.15	8.96	100
	NP3b	15.25	8.85	90
	NP2	15.40	9.20	29
	NP1	15.10	8.71	4.0
	SDS	15.42	8.70	76
6	H_2O	16.41	13.98	—
	NP3a	15.74	12.80	80
	NP3b	15.65	12.88	40
	SDS	15.81	12.72	37

[a] K_{eq} refers to the organic chain concentration. [b] Taken from ref. 17. [c] Taken from ref. 18. [d] Taken from ref. 14. * These NPs present a shorter PEG composed of 4 oxoethylene units,[13,14] and have an average core diameter of 1.6 nm. ** As **NP1*** with an average core size of 3.4 nm.[13,14]

dominant species. In Table 2 are reported the spectroscopic parameters for the nitroxides partitioned in the monolayers.

Inspection of Table 2 shows that both the value of a(N) and of $a(2H_\beta)$ decrease considerably when the aminoxyl radical is located in the hydrophobic region of the monolayer, giving rise to significant differences in the resonance fields for the $M_I(2H_\beta) = \pm 1$ lines of the two spectra. The reduction of a(N), already reported in previous studies carried out with different nitroxide radicals,[19] has been attributed to the larger weight in media of low polarity of the nitroxide mesomeric forms in which the unpaired electron is localized on the oxygen rather on the nitrogen atom.

The reduction of a(N) remains approximately constant by changing the nature of the probe and the monolayer. This suggests that the polarity of the environment surrounding the nitroxide function is similar for all radicals. The N–O group is deeply inside the monolayer with the polar O–H group presumably close to the hydrophilic region of the monolayer and the aromatic ring in the fluorinated or lipophilic part. The partition of the probe in the environment of the monolayer gives rise to a reduction also of the β-proton splitting, with the result that the resonance fields for the $M_I(2H_\beta) = \pm 1$ lines of the

free and included species are significantly different. This allows an easy determination of the partition constants K_{eq} (see Table 2) which were obtained by plotting the ratio between the concentrations of the nitroxide dissolved in the monolayer and the free species in water.

We also determined the partition constants of probes **1**, **2**, **5** and **6** in the hydrophobic environment of sodium dodecyl sulfate (SDS) micelles (see Table 2). Comparison of these data with those obtained with hydrogenated and fluorinated monolayer-protected nanoparticles allowed us to extract the hydrophobic contribution in the value of K_{eq} for the fluorinated nitroxide probes. With nanoparticles **NP1** and **NP2**, probes **1**, **4** and **6** did not display significant binding, as it was observed in our previous studies of radical probe **1** with nanoparticles **NP1***, structurally related to **NP1** but featuring a shorter PEG unit.[13] In contrast, all of the probes in the panel displayed measurable affinities for nanoparticles **NP3a** and **NP3b**, with binding constants increasing with the increase of the hydrophobicity (probes **1**, **2** and **3**) and of the fluorine content of the probes (probes **4–6**). Moreover, the binding constants increase with the increasing size of the nanoparticles.

Inspection of Table 3 reporting the comparison of the equilibrium constants determined for the partition of probe **2** in the monolayer of **NP1**, **NP2** and **NP3a** allows extraction of some relevant information on the effect exerted by fluorinated monolayers on the binding of hydrogenated probes.

The binding constant of **2** with the fluorinated monolayer of **NP2** and **NP3a** is 2.6 and 7.2 times higher than the binding constant measured for the interaction with the hydrogenated monolayer of **NP1**, Table 3. Given the structural similarity of the nanoparticles' monolayer, the increase in binding affinity must be the result of a favourable interaction of **2** with the fluorous regions of **NP2** and **NP3a**, *vide infra*.

Comparing the interaction of probes **2** and **5** with nanoparticles **NP1**, **NP2**, and **NP3a**, Table 3, allows us to assess the relevance of fluorophilic interactions between fluorinated guests and fluorinated hosting monolayers. For probe **5** in the presence of the hydrogenated monolayer of **NP1** we observed a 1.8-fold increase in the value of K_{eq} with respect to that obtained for probe **2** and the same nanoparticles. This increase is very similar to that observed with SDS micelles (1.7, see Table 3) where only hydrophobic interactions are expected to be important in determining the affinity of the probe.[20] Thus the observed increase should be related only to an increase of the hydrophobicity of **5** compared to **2**.

In contrast, with the fluorinated monolayer of **NP2** we observed a 5.1-fold increase in the value of K_{eq} with respect to that obtained for probe **2** and the same nanoparticles (K_{eq}(F)/K_{eq}(H) in Table 4). The relevance of fluorophilic interactions is also evident in comparing the binding constants of the pairs of structurally similar probes **5**, **2** and **6**, **1** with **NP3a**. The binding constant of **5** (K_{eq} = 100 M^{-1}) is 6.25 times higher than the binding constant of **2** (K_{eq} = 16 M^{-1}) and the binding constant of fluorinated probe **6** (K_{eq} = 80 M^{-1}) is almost thirteen times higher than the binding constant of **1** (K_{eq} = 6.2 M^{-1}).

Table 4 Binding constants of probes **1**, **2**, **5** and **6** for the monolayer of nanoparticles **NP1–NP3a** and ratios of the binding constants of the fluorinated and hydrogenated probes for each nanoparticle system

	K_{eq} (**2**)/M^{-1}	K_{eq} (**5**)/M^{-1}	K_{eq} (**1**)/M^{-1}	K_{eq} (**6**)/M^{-1}	K(F)/K(H)
NP1	2.2	4.0	—	—	K(**5**)/K(**2**) = 1.8
NP2	5.7	29	—	—	K(**5**)/K(**2**) = 5.1
NP3a	16	100	6.2	80	K(**5**)/K(**2**) = 6.2
					K(**6**)/K(**1**) = 12.9

A considerable increase (7.2 times) of the binding affinity of **5** for the fluorinated monolayer of **NP2** is also observed with respect to the hydrogenated monolayer of **NP1**. Similarly, when the interaction of **5** with **NP3a** was considered (K_{eq} = 100 M^{-1}), a 25-fold increase with respect to the interaction of **5** with **NP1** was obtained. Previous data on the complexation of probe **3** with nanoparticles **NP1*** and **NP1****, structurally similar to **NP1** and of the same diameter as **NP3b** show that also in this case the complexation of hydrogenated guests is favoured in fluorinated monolayers, Table 2.

The behaviour observed with **NP3a** is paralleled by the smaller **NP3b** with a core diameter of 1.4 nm protected with the same thiolate ligand. However, in this case a small reduction in the binding constants was observed, with clear indication that reducing the inter-ligand available room as in **NP3a** tightens the binding of the guest. Our previous studies on nanoparticles **NP1*** and **NP1**** that differ from the systems under analysis for the presence of a shorter oxoethylene unit and for the absence of the fluorinated moiety displayed an opposite trend, with smaller particles acting as better hosting systems. In this case the hydrophobic interactions occurring in the conformationally rigid hydrophobic region of the monolayer dominate the binding. Instead, in the case of **NP3a** and **NP3b**, the binding is dominated by the interactions with the conformationally flexible perfluoropolyether units of the monolayer. The higher the packing of the ligands, the smaller conformational rearrangement is necessary to achieve optimal binding.

Among the nanoparticles featuring a fluorous monolayer, the binding constants for probes **2** and **5** increase going from

Table 3 Binding constants of probes **2** and **5** for the monolayer of nanoparticles **NP1–NP3a** and ratios of the binding constants determined for the two probes with the three nanoparticles investigated

Probe	K_{eq}/M^{-1} (**NP1**)	K_{eq}/M^{-1} (**NP2**)	K_{eq}/M^{-1} (**NP3a**)	K_{eq}/M^{-1} (SDS)	K(**NP2**)/K(**NP1**)	K(**NP3a**)/K(**NP2**)	K(**NP3a**)/K(**NP1**)
2	2.2	5.7	16	44	2.6	2.8	7.2
5	4.0	29	100	76	7.2	3.4	25

NP2 to **NP3a**. The same trend was observed with probe **3**: K_{eq} = 593 M^{-1} for **NP3b**, while for **NP2** the binding constant was K_{eq} = 176 M^{-1}.

All of these data suggest that the interaction of hydrogenated probes with fluorinated nanoparticles is more favourable than the interaction of the same probes with the hydrogenated monolayer of structurally similar nanoparticles. The highest gain in binding affinity is, however, achieved when fluorinated probes interact with fluorinated monolayers. These effects result from the superimposition of different contributions that clearly add to the simple hydrophobic interaction between hydrogenated guests and hydrogenated monolayers. The stabilization of the fluorinated guests in the hydrophobic environment of the monolayer with release of the high energy water molecules of their solvation shell to the solvent bulk is an important driving force. This adds to the fluorophilic interactions[21,22] established between fluorinated guests and fluorinated monolayers. Geometric considerations also suggest that in the case of **NP2** the enhanced binding affinity may be due to the larger cross-section of fluorinated alkyl chains with respect to hydrogenated ones. In proximity of the gold surface they are both quite rigid, allowing a larger space for the probe to be hosted in the fluorinated monolayer as graphically represented in Fig. 2 with a red cone.

We may speculate that an additional contribution to the binding might be due to the formation of weak interactions involving halogen bonds[23] as F–π with the aromatic ring of the probe or between the fluorinated probes and the oxygen atoms of the PEG chains.

The increase of binding constants determined for the nanoparticle systems **NP3a** and **NP3b** with respect to **NP2** is somewhat counterintuitive since the more flexible fluorinated region of the monolayer of **NP3a** could be considered not pre-organized to serve as a suitable host. Indeed we propose that upon complexation of the hydrogenated/fluorinated guests, the perfluoropolyether moieties of **NP3a** and **NP3b** may undergo a structural reorganization strengthening the binding of the guests. This hypothesis is supported by the observation that larger nanoparticles with reduced inter-ligand distances act as better hosts than smaller nanoparticles.

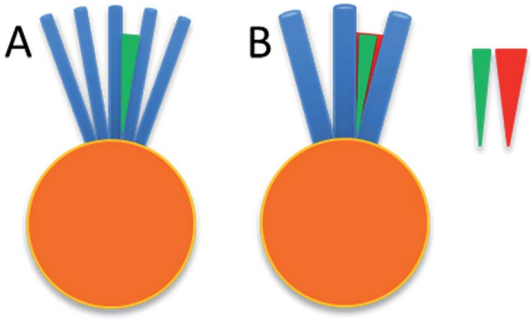

Fig. 2 Graphical representation of the alkyl portion of hydrogenated ligands in NP1 (A) and fluorinated alkyl chains of NP2 (B) and the space illustrated as a green cone for NP1 and a red cone for NP2.

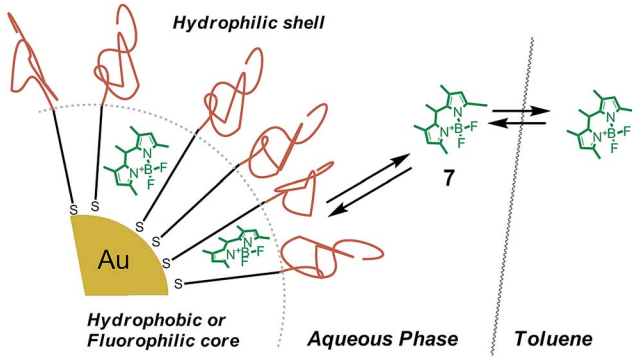

Fig. 3 Representation of the equilibria involved in the phase transfer of 7 in the presence of nanoparticles.

Release studies by fluorescence spectroscopy

Preliminary kinetic studies aimed at characterizing the interaction between the monolayer of **NP1**, **NP2**, **NP3a** and **NP3b** on small organic molecules were undertaken by assessing the effect of the monolayer passivating the nanoparticles on the phase transfer rate of the hydrophobic fluorescent BODIPY dye 7, Scheme 2, from an aqueous solution containing nanoparticles to a toluene layer, Fig. 3. Briefly, an aliquot of aqueous solution of 7 (0.5 mL, 1.68 × 10^{-7} M) was added to dry NP in a fluorimetric cuvette, then 2 mL of toluene was slowly added.§

The fluorescence intensity of dye released in toluene was monitored under gentle stirring. When the dye is entrapped into the monolayer its fluorescence is quenched by the NP, the fluorescence was only observed in the toluene layer upon dye transfer.

In these experiments, the concentrations of both nanoparticles and 7 were in the lower micromolar range with a 7/NP molar ratio equal to: 0.39 for **NP1**; 0.27 for **NP2**; 0.67 for **NP3a** and 0.15 for **NP3b**. In the absence of nanoparticles, the phase transfer of 7 is described by an approximately first order process with a rate constant (k_1 in Table 5) of 0.03 s^{-1}. Conversely, when nanoparticles **NP1**, **NP3a** and **NP3b** were tested, clear biphasic kinetics where a fast process precedes a slower one were obtained, Fig. 4. Fitting of the experimental data with a biexponential model allowed estimation of the observed rate constants for the two processes referred to as k_1 and k_2 in Table 5. The first process occurs with a rate constant closely matching that measured for the phase transfer of 7 in the absence of nanoparticles. The second process takes place with a much smaller rate constant, slowing down the overall rate for the transfer of 7 from the aqueous to the toluene layer. Instead, for nanoparticles **NP2**, the process was not clearly biphasic but resembled a simple first order process though with evident deviation from the ideal behaviour. Initial rate analysis allowed determination of the rate constant for the process that was 5 × 10^{-3} s^{-1}, 6 times smaller than the first order rate constant measured in the absence of nanoparticles.

§ **NP1**, **NP2**, **NP3a** and **NP3b** are soluble in water but insoluble in toluene.

Table 5 Kinetic parameters for the phase transfer of the BODIPY dye 7 in the presence and absence of NP1, NP2, NP3a and NP3b

Nanoparticles	k_1/s^{-1}	k_2/s^{-1}	[NP]/μM	[7]/μM
None	0.03	—	—	0.168
NP1	0.02	2×10^{-4}	0.426	0.168
NP2	5×10^{-3}	—	0.632	0.168
NP3a	0.02	5×10^{-4}	0.229	0.153
NP3b	0.03	4×10^{-4}	1.15	0.168

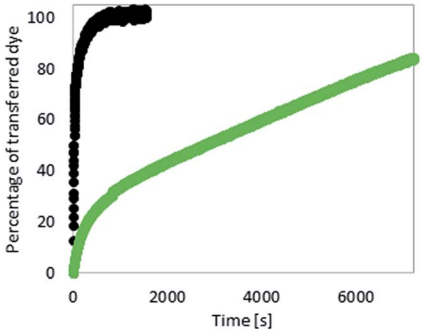

Fig. 4 Kinetic profiles for the phase transfer of 7 from an aqueous phase to the toluene layer in the absence (black line) and in the presence of NP3a (green line).

The observation of a clearly biphasic regime in the case of **NP1**, **NP3a** and **NP3b** strongly suggests the existence of two different populations of 7 that differ for their ease of phase transfer. Since the first fast process observed takes place with a rate constant matching the rate constant measured for the phase transfer of 7 in the absence of nanoparticles, we put forth the hypothesis that this fast process pertains to the transfer of the free 7 present in solution.

Therefore the second, slow, process of the observed biphasic regime, besides the actual values of k_2, is tentatively assigned to the phase transfer of the BODIPY dye 7 interacting with the monolayer of the nanoparticles.

Conclusions

ESR studies employing the hydrogenated or fluorinated radical probes **1–6** and hydrogenated and fluorinated homoligand nanoparticles **NP1**, **NP2**, **NP3a** and **NP3b** allowed us to establish that fluorinated monolayers act as hosting systems with enhanced binding affinities for both hydrogenated and fluorinated radical probes with respect to nanoparticles featuring hydrogenated monolayers. The intervention of fluorophilic interactions in the binding events is clearly discernible when hydrogenated and fluorinated probes of similar structures are compared. Probe **5** featuring a *p*-trifluoromethyl group is complexed by the monolayer of **NP3a**, 6 times stronger than probe **2**, that features a *p*-methyl group on the aryl ring. Probe **6** featuring a perfluorinated aromatic ring is complexed 13 times stronger than its hydrogenated counterpart **2**. These interactions that may also comprise the formation of weak halogen bonds add to hydrophobic interactions determining an overall increased binding affinity. Most notably hydrophobic small molecules are complexed by the flexible fluorinated monolayers of **NP3a** and **NP3b** with higher affinity with respect to the rigid fluorinated monolayer of **NP2** or the hydrophobic monolayer of **NP1**. Preliminary studies aimed at characterizing the effect of nanoparticles **NP1**, **NP2**, **NP3a** and **NP3b** on the phase transfer of the hydrophobic BODIPY dye 7 evidenced that all of the nanoparticles are able to slow down the rate of phase transfer as the result of the complexation equilibria involving the dye and the nanoparticles.

Experimental

Gold nanoparticles **NP1**, **NP2**, **NP3a** and **NP3b** were prepared according to our previously reported procedures[13,14,16,17] using thiols **8**, **9** and **10**, Scheme 3; the synthesis of thiol **8** is reported in the ESI;† the synthesis of thiols **9** and **10** has been described elsewhere.[17,18] For the synthesis of **NP2**, sodium thiolate of compound **9** was used owing to the low nucleophilicity of its sulfidryl group. Amines **1H–3H** were prepared according to our previously reported procedure.[13]

Synthesis of NP1

$HAuCl_4 \cdot 3H_2O$ (78.5 mg, 0.199 mmol) and 40 mL of deoxygenated MilliQ water were introduced into a 250 mL round-bottom flask. To the pale yellow solution, thiol **8**, see ESI,† (94 mg, 0.133 mmol) dissolved in 80 mL of deoxygenated methanol was added. The mixture was left to stir for 30 minutes, while its colour faded on standing. The solution was cooled to 0 °C and keeping at that temperature for 30 minutes, further fading was observed. A solution of $NaBH_4$ 0.1 M (19.9 mL, 1.99 mmol) in MilliQ water was added in 210 seconds, the reaction mixture turned immediately reddish-brown, and the mixture was stirred at 0 °C for 30 minutes and then at room temperature for 2 hours. The solvent was removed under reduced pressure without heating above 35 °C. The solid was washed copiously with diethyl ether and purified by gel permeation chromatography (Sephadex LH-20, methanol) and by dialysis giving 41 mg of nanoparticles. ^{1}H-NMR (400 MHz, CD_3OD) δ: 1.4 (br, CH_2); 1.6 (br, CH_2); 2.25 (br, CH_2CO); 3.34 (br, CH_3O); 3.4–3.75 (br, CH_2O). UV-Vis (MeOH, $c = 0.1$ mg mL^{-1}): $\lambda_{max} = 531$ nm. TEM: average diameter = 3.45 nm; $\sigma = 0.61$ nm; $N = 400$. TGA: 39.5%. Average composition: $Au_{1414}(SR)_{270}$.

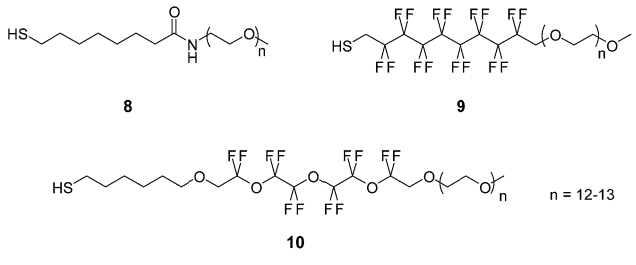

Scheme 3 Structures of the thiols used in the preparation of nanoparticles NP1, NP2, NP3a and NP3b.

Synthesis of NP2

Thiol **9** (79.1 mg, 7.6×10^{-5} mol) was dissolved in 1.2 mL of dry and deoxygenated methanol, under an argon atmosphere. To the mixture, 0.446 mL (2.23×10^{-4} mol, 3 equiv.) of 0.5 M sodium methoxide in methanol was added. The solution was stirred for one hour. Before use the solution was diluted with 10.4 mL of dry and deoxygenated methanol.

$HAuCl_4 \cdot 3H_2O$ (75 mg, 1.90×10^{-4}) was dissolved in 40 mL of deoxygenated MilliQ water, under an argon atmosphere and poured into a 100 mL round bottom flask. A solution of sodium 2,2,3,3,4,4,5,5,6,6,7,7,8,8,9,9-hexadecafluoro-10-(methoxy-PEG550)decan-1-thiolate (0.10 g, 9.59×10^{-5}) in dry and deoxygenated methanol (15 mL) was added to the mixture through a double-tipped needle under an argon atmosphere. The solution was stirred at room temperature for 1 hour. Then a $NaBH_4$ powder (83 mg, 2.19×10^{-3}mol) dissolved in 5.5 mL (15.2 mg mL^{-1}) of deoxygenated MilliQ water was added dropwise in 15 minutes. The solution colour turned reddish suggesting the formation of protected nanoparticles. The mixture was left stirring for 3 h, and then the solvent was removed under reduced pressure. The residue was transferred into a centrifuge tube, dispersed in diethyl ether, and repeatedly washed (4 × 15 mL) by centrifugation at 4000 rpm to remove unbound thiols. The precipitate was recovered as a dark brown solid, 42 mg. ^{1}H-NMR (CD_3OD, 500 MHz) δ: 3.38 (br, CH_3O), 3.48–3.77 (br, CH_2O), 4.10 (br, CF_2CH_2O). UV-Vis (MeOH, $c = 0.1$ mg mL^{-1}): $\lambda_{max} = 513$ nm TEM: average diameter = 2.96 nm; $\sigma = 0.63$ nm; $N = 392$. TGA: 39%. Average composition: $Au_{976}(SR)_{120}$.

Synthesis of NP3a

$HAuCl_4 \cdot 3H_2O$ (68 mg, 0.173 mmol) and 40 mL of deoxygenated MilliQ water were introduced into a 250 mL round-bottom flask. To the pale yellow solution, thiol **10**, see ESI† (121 mg, 0.114 mmol), dissolved in 40 mL of deoxygenated methanol was added. The mixture was left to stir for 30 minutes, while its colour faded on standing. The solution was cooled to 0 °C and keeping at that temperature for 30 minutes, further fading was observed. A solution of $NaBH_4$ 0.1 M (19 mL, 1.9 mmol) in MilliQ water was added in 210 seconds, the reaction mixture turned immediately reddish-brown, and the mixture was stirred at 0 °C for 30 minutes and then at room temperature for 2 hours. The solvent was removed under reduced pressure without heating above 35 °C. The solid was washed copiously with diethyl ether and purified by gel permeation chromatography (Sephadex LH-20, methanol) and by dialysis giving 63 mg of nanoparticles. ^{1}H-NMR (500 MHz, CD_3OD): $\delta = 4.04$ (br); 3.87 (br); 3.76 (br), 3.64 (br), 3.30 (s, 3H, OCH_3); 1.60 (br), 1.40 (br) ppm. UV-Vis (MeOH, $c = 0.1$ mg mL^{-1}): $\lambda_{max} = 514$ nm. TEM: x_m average diameter = 2.97 nm; $\sigma = 0.73$ nm; $N = 283$. TGA: 61.7%. Average composition: $Au_{976}(SR)_{187}$.

Synthesis of NP3b

$HAuCl_4 \cdot 3H_2O$ (78.6 mg, 0.199 mmol) and 50 mL of MilliQ water were introduced into a 250 mL round-bottom flask. To the pale yellow solution, thiol **10**, see ESI† (422 mg, 0.399 mmol), dissolved in 50 mL of deoxygenated methanol was added. The solution turned immediately reddish-brown; the mixture was left to stir for 30 minutes, while its color faded on standing. The solution was cooled to 0 °C and keeping at that temperature for 30 minutes, further fading was observed. A solution of $NaBH_4$ 0.1 M (22 mL, 2.19 mmol) in MilliQ water was added in 10 seconds, the reaction mixture turned immediately dark-brown, and the mixture was stirred at 0 °C for 30 minutes and then at room temperature for 2 hours. The solvent was removed under reduced pressure without heating above 35 °C. The residue was concentrated to a small volume and treated with diethyl ether in order to precipitate the nanoparticles. The black solid was washed copiously with diethyl ether and purified by gel permeation chromatography (Sephadex LH-20, methanol) and by dialysis giving 165 mg of nanoparticles. ^{1}H-NMR (500 MHz, CD_3OD): $\delta = 4.04$ (br); 3.87 (br); 3.76 (br), 3.64 (br), 3.30 (s, 3H, OCH_3); 1.60 (br), 1.40 (br) ppm. UV-Vis (methanol): $\lambda_{max} = 383$ nm. TEM: average diameter = 1.41 nm; $\sigma = 0.28$ nm; $N = 283$. TGA: 84%. Average composition: $Au_{100}(SR)_{60}$.

General procedure for the preparation of amines 4H–6H

A toluene solution (100 mL) of 2-amino-2-methyl-1-propanol (10 mmol) and the appropriate substituted benzaldehyde (10 mmol) was stirred and heated under reflux for 10 h. During the reaction water was removed using a Dean–Stark apparatus. The solution was cooled and evaporated under reduced pressure to afford the corresponding imine (yield 90–95%). The imine (9 mmol) was then dissolved in a 1 : 1 solution of THF–methanol (80 mL), and stirred at room temperature for 2 h in the presence of $NaBH_4$ (10 mmol). Another portion of $NaBH_4$ was then added to the reaction mixture (10 mmol) and the solution was stirred further for 16 h. The solution was treated with HCl 6 N (50 mL) and the solvent was removed by evaporation under reduced pressure. The residue was treated with aqueous NaOH 5 N (100 mL) and extracted with CH_2Cl_2 (100 mL × 3). The organic phase was washed with water (100 mL), before being dried ($MgSO_4$) and evaporated under reduced pressure. The product was purified by column chromatography (eluent petroleum diethyl ether–ethyl acetate 1/1 to 1/5, NH_3 1%, v/v) to give the white solid amine (yield 85–90%).

4H. Elemental analysis for $C_{11}H_{16}FNO$: calc.: C, 66.98; H, 8.18; F, 9.63; N, 7.10; O, 8.11; found: C, 66.90; H, 8.20; F, 9.61; N, 7.14; ^{1}H-NMR (600 MHz, $CDCl_3$) δ: 7.29 (q, $J = 7.2$ Hz, 2H), 7.00 (t, $J = 12.9$ Hz, 2H), 3.65 (s, 2H), 3.34 (s, 2H), 1.14 (s, 6H); GC-MS (m/z): 179 ($M^+ - 18$, 10), 109 ($M^+ - 88$, 100); ESR parameters of the corresponding nitroxide **4**: see Table 2.

5H. Elemental analysis for $C_{11}H_{12}F_5NO$: calc.: C, 49.08; H, 4.49; F, 35.29; N, 5.20; O, 5.94; found: C, 48.99; H, 4.52; F, 35.28; N, 5.14; ^{1}H NMR (600 MHz, $CDCl_3$) δ 3.80 (s, 2H), 3.38 (s, 2H), 1.15 (s, 6H); GC-MS (m/z): 251 ($M^+ - 18$, 10), 236 ($M^+ - 33$, 20), 181 ($M^+ - 88$, 100); ESR parameters of the corresponding nitroxide **5**: see Table 2.

6H. Elemental analysis for $C_{12}H_{16}F_3NO$: calc.: C, 58.29; H, 6.52; F, 23.05; N, 5.66; O, 6.47; found: C, 58.33; H, 6.49; F, 23.15; N, 5.69; ^{1}H-NMR (600 MHz, $CDCl_3$) δ 7.57 (d, $J = 12$ Hz, 2H), 7.45 (d, $J = 12$ Hz, 2H), 3.74 (s, 2H), 3.36 (s, 2H), 1.15 (s, 6H); GC-MS

(m/z): 229 ($M^+ - 18$, 10), 214 ($M^+ - 33$, 15), 159 ($M^+ - 88$, 100); ESR parameters of the corresponding nitroxide **6**: see Table 2.

ESR measurements

Radicals **1b–6b** were generated by mixing 0.5 μL of a methanol solution containing the corresponding amine (0.05 M) and 0.5 μL of a water solution containing Oxone (0.05 M) with 50 μL of a water solution containing variable amounts of NPs. Samples were transferred in capillary tubes (diameter 1 mm) and then placed inside the thermostatted cavity of the ESR spectrometer. ESR spectra were recorded using a Bruker ELEXYS E500 spectrometer equipped with an NMR gaussmeter for field calibration and a microwave frequency counter for g-factor determination.

The instrument settings were as follows: microwave power 5.0 mW, modulation amplitude 0.05 mT, modulation frequency 100 kHz, conversion time 164 ms. Digitized ESR spectra were transferred to a personal computer for analysis using digital simulations carried out with a program developed in our laboratory and based on a Monte Carlo procedure. The input data for the program are the number of nonequivalent nuclei, the hyperfine splitting constants of the free and included radical, the intrinsic line width in the absence of exchange, and the rate constants for the exchange process.

General procedure for delivery studies by fluorescence

An aliquot of aqueous solution of BODIPY dye **7** (0.5 mL) was added to dry nanoparticles in a fluorimetric cuvette, and then 2 mL of toluene were added. The fluorescence intensity of dye release in toluene was monitored at 509 nm under stirring, using an excitation wavelength of 500 nm and an averaging time of 0.5 s.

Delivery study of NP1–7. 0.1 mg of dry **NP1** and 0.5 mL of a 1.68×10^{-7} M solution of **7** in water.

Delivery study of NP2–7. 0.1 mg of dry **NP2** and 0.5 mL of a 1.68×10^{-7} M solution of **7** in water.

Delivery study of NP3a–7. 0.05 mg of dry **NP2** and 0.5 mL of a 1.53×10^{-7} M solution of **7** in water.

Delivery study of NP3b–7. 0.048 mg of dry **NP3b** and 0.5 mL of a 1.68×10^{-7} M solution of **7** in water.

Acknowledgements

Italian Ministry of Health: project GR-2009-1579849; FIRB prot. RBAP11ETKA, MIUR: Project MULTINANOITA; University of Trieste: FRA 2011; University of Bologna (Finanziamenti di Ateneo alla Ricerca di Base, SLaMM Project).

Notes and references

1 K. Riehemann, S. W. Schneider, T. A. Luger, B. Godin, M. Ferrari and H. Fuchs, *Angew. Chem., Int. Ed.*, 2009, **48**, 872–897.
2 A. Z. Wang, R. Langer and O. C. Farokhzad, *Annu. Rev. Med.*, 2012, **63**, 185–198.
3 Y. Chen, H. Chen and J. Shi, *Adv. Mater.*, 2013, **25**, 3144–3176.
4 C. S. Kim, G. Y. Tonga, D. Solfiell and V. M. Rotello, *Adv. Drug Delivery Rev.*, 2013, **65**, 93–99.
5 A. M. Alkilany, L. B. Thompson, S. P. Boulos, P. N. Sisco and C. J. Murphy, *Adv. Drug Delivery Rev.*, 2012, **64**, 190–199.
6 P. Ghosh, G. Han, M. De, C.-K. Kim and V. M. Rotello, *Adv. Drug Delivery Rev.*, 2008, **60**, 1307–1315.
7 F. Wang, Y. C. Wang, S. Dou, M. H. Xiong, T. M. Sun and J. Wang, *ACS Nano*, 2011, **5**, 3679–3692.
8 L. Hosta, M. Pla-Roca, J. Arbiol, C. López-Iglesias, J. Samitier, L. J. Cruz, M. J. Kogan and F. Albericio, *Bioconjugate Chem.*, 2008, **20**, 138–146.
9 S. S. Agasti, A. Chompoosor, C.-C. You, P. Ghosh, C. K. Kim and V. M. Rotello, *J. Am. Chem. Soc.*, 2009, **131**, 5728–5729.
10 R. Hong, G. Han, J. M. Fernández, B.-J. Kim, N. S. Forbes and V. M. Rotello, *J. Am. Chem. Soc.*, 2006, **128**, 1078–1079.
11 C. K. Kim, P. Ghosh, C. Pagliuca, Z.-J. Zhu, S. Menichetti and V. M. Rotello, *J. Am. Chem. Soc.*, 2009, **131**, 1360–1361.
12 Y. Cheng, A. C. Samia, J. D. Meyers, I. Panagopoulos, B. Fei and C. Burda, *J. Am. Chem. Soc.*, 2008, **130**, 10643–10647.
13 M. Lucarini, P. Franchi, G. F. Pedulli, P. Pengo, P. Scrimin and L. Pasquato, *J. Am. Chem. Soc.*, 2004, **126**, 9326–9329.
14 M. Lucarini, P. Franchi, G. F. Pedulli, C. Gentilini, S. Polizzi, P. Pengo, P. Scrimin and L. Pasquato, *J. Am. Chem. Soc.*, 2005, **127**, 16384–16385.
15 *Fluorine in Medicinal Chemistry and Biology*, ed. I. Ojima, Blackwell Publishing, Chippenham, Wiltshire (UK), 2009.
16 P. Pengo, S. Polizzi, M. Battagliarin, L. Pasquato and P. Scrimin, *J. Mater. Chem.*, 2003, **13**, 2471–2478.
17 M. Boccalon, P. Franchi, M. Lucarini, J. J. Delgado, F. Sousa, F. Stellacci, I. Zucca, A. Scotti, R. Spreafico, P. Pengo and L. Pasquato, *Chem. Commun.*, 2013, **49**, 8794–8796.
18 C. Gentilini, F. Evangelista, P. Rudolf, P. Franchi, M. Lucarini and L. Pasquato, *J. Am. Chem. Soc.*, 2008, **130**, 15678–15682.
19 P. Franchi, C. Casati, E. Mezzina and M. Lucarini, *Org. Biomol. Chem.*, 2011, **9**, 6396–6401.
20 G. Brigati, P. Franchi, M. Lucarini, G. F. Pedulli and L. Valgimigli, *Res. Chem. Intermed.*, 2002, **28**, 131–141.
21 J. W. Ward, R. Li, A. Obaid, M. M. Payne, D.-M. Smilgies, J. E. Anthony, A. Amassian and O. D. Jurchescu, *Adv. Funct. Mater.*, 2014, **24**, 5052–5058.
22 M. S. Pavan, K. Durga Prasad and T. N. G. Row, *Chem. Commun.*, 2013, **49**, 7558–7560.
23 G. R. Desiraju, P. S. Ho, L. Kloo, A. C. Legon, R. Marquardt, P. Metrangolo, P. Politzer, G. Resnati and K. Rissanen, *Pure Appl. Chem.*, 2013, **85**, 1711–1713.